

On the saturation of acoustic mode frequencies at high solar activity

M. Cristina Rabello Soares, [★]

Physics Department, Universidade Federal de Minas Gerais, Belo Horizonte, MG 31270-901, Brazil

Accepted XXX. Received YYY; in original form ZZZ

ABSTRACT

Acoustic mode frequencies obtained by applying spherical harmonic decomposition to HMI, MDI and GONG observations were analysed throughout the solar cycle. Evidence of a deviation from a linear relation with solar radio flux was found indicating a saturation effect at high solar activity. The Gompertz model, which is one of the most frequently used sigmoid functions to fit growth data, is used. It is shown that its fitting to MDI and GONG data are statistically significant and a median saturation of four-hundred sfu is estimated. This saturation level is 50% larger than any obtained in the last century, hence the small effect observed in the minimum-to-maximum frequency shift. However, as shown here, it should not be disregarded.

Key words: Sun: activity – Sun: helioseismology – Sun: oscillations – stars: activity

1 INTRODUCTION

The Sun undergoes periods of strong and weak activity over the course of 11 years, which is most commonly seen as a cyclic variation in the number of sunspots present in the solar surface. The cycles have been observed for the last 400 years and, starting at mid-18th century, the cycles have been labelled with a number. We are currently moving into cycle 25. The origin of the eleven-year solar magnetic activity cycle is still not completely understood. There are yet questions on how the magnetic fields are built inside the Sun. The results of dynamo simulations are still somewhat dependent on numerical parameters that are orders of magnitude away from those in real stars (see review by [Brun & Browning 2017](#)). A number of tracers quantifying solar activity have been used given by different observables that are linked to different aspects of solar activity and to different heights in the solar atmosphere. These indices are usually highly correlated to each other due to the predominant eleven-year cycle, apart from small differences on short- or long-term scale (see review by [Usoskin 2017](#)).

The frequencies of the acoustic modes, that propagate inside the Sun, vary with the solar activity cycle ([Woodard & Noyes 1985](#); [Libbrecht & Woodard 1990](#); [Chaplin et al. 2001](#), and references within). Although the variation in the mode frequencies is small ($\lesssim 0.1\%$), it is well correlated with several solar indices (see, for example, [Jain et al. 2009](#); [Broomhall & Nakariakov 2015](#), and references within). In fact, the seismic proxy for magnetic activity has been used to reveal an activity cycle similar to that

of the Sun on other stars ([García et al. 2010](#); [Kiefer et al. 2017](#); [Santos et al. 2018](#), and references within). Despite the progress in understanding the source of mode frequency variation with activity ([Gough 1990](#); [Goldreich et al. 1991](#); [Li et al. 2003](#); [Dziembowski & Goode 2005](#); [Mullan et al. 2007](#), among others), the picture is not completely clear. This work adds to clarify this as it contributes to quantifying the observed behaviour of mode frequency variation with solar activity. Here it is shown that the frequency increase with solar activity is not linear, but it is better represented by a sigmoid function, where the frequency increase reaches a maximum.

2 DATA

There are three sets of helioseismic data available that cover at least a broad part of a solar cycle and are not restricted to very low l modes. I analyse all three.

The Michelson Doppler Imager (MDI) onboard the Solar and Heliospheric Observatory (SOHO) has a 1024×1024 pixel CCD with a dopplergram obtained every 60 seconds ([Scherrer et al. 1995](#)). In the Medium- l Program (also called the Structure Program), the image is subsampled to a resolution that is only one-fifth of the full-disk data and cropped to 90% of the average solar radius. Mode parameters for 72-day long time series are provided by the global helioseismology pipeline (see [Larson & Schou 2018](#), for details). The data was obtained almost continuously from May 1996 to April 2011.

Helioseismic and Magnetic Imager (HMI), designed to succeed MDI, was launched onboard the Solar Dynamics

[★] E-mail: cristina@fisica.ufmg.br

Observatory (SDO) in February 2010 (Schou et al. 2012). It has a 4096×4096 pixel CCD and observes a dopplergram every 45 seconds. HMI observes the Doppler shift of Fe I 6173 Å spectral line, while MDI observed the Ni I 6768 Å line. HMI samples the acoustic modes at a slightly lower height in the solar atmosphere than MDI (Fleck et al. 2011). The mode parameters for 72-day long time series are provided by the global helioseismology pipeline, see Larson & Schou (2018) for details and for a comparison with MDI. I analysed data obtained from April 2010 to June 2017.

The Global Oscillation Network Group (GONG), consisting of six instruments around the world, observes the Doppler shift at the same line and at the same sampling time as MDI (Harvey et al. 1996). Its 256×256 pixel CCD was replaced by a 1024×1024 one in 2001. The mode parameters for 36-day long time series are provided by the GONG pipeline (Hill et al. 1996). I use the central frequency obtained using Clebsch-Gordon coefficients after fitting each individual mode (radial order n , spherical degree l and azimuthal order m). In the MDI and HMI pipeline, the multiplet ($2l + 1$ m 's) are fitted together (Larson & Schou 2015). Unfortunately, the six ground stations are not enough to get a duty cycle as high as MDI and HMI space missions. HMI has a duty cycle larger than 0.96 (Larson & Schou 2018). GONG's duty cycle varies from 0.67 to 0.96, where 98% is lower than 0.95 (Kiefer et al. 2018), while only 24% of MDI's are smaller than 0.95 (Larson & Schou 2015). For comparison purposes, only GONG data at the same time period as MDI is used.

As a physical indicator of the solar activity, I will use the daily measurements of the integrated emission from the solar disc at 2.8 GHz (corresponding to a 10.7 cm wavelength) provided by the National Resources Canada (NRC) Space Weather (Covington 1969; Tapping 1987). The solar flux density (represented in this work as ϕ) is measured in solar flux units (sfu), where $1 \text{ sfu} = 10^{-22} \text{ W} \cdot \text{m}^{-2} \cdot \text{Hz}^{-1}$. The solar radio flux has contributions from three sources: active regions cores, in and around plages and outside active regions, and a background from the quiet Sun (Tapping 1987). The quiet Sun radio flux is usually at $65 \pm 2 \text{ sfu}$ (Schonfeld et al. 2015, and references within). I use the adjusted value corrected for variations in the Earth-Sun distance. The daily values are averaged over each instrument time series (72-day for MDI and HMI, and 36-day for GONG). Figure 1 shows the averaged radio flux during MDI, GONG, and HMI observations. Cycle 24 is approximately 0.7 smaller than Cycle 23.

3 ANALYSIS

There is a very high linear correlation of the mode frequency variation with the solar activity where Pearson's linear coefficient is very close to one (Jain et al. 2009). However, in my previous work, I found evidence of a quadratic relation indicating a saturation effect at high solar activity (Rabello-Soares 2011). In fact, Figure 2 shows that the slope decreases as the activity increases. I fitted a straight line to the individual mode frequencies observed by MDI with radio fluxes smaller than their mid-point ('low') and with fluxes larger than their mid-point ('high'). In the figure, it is plotted the relative difference between these two slopes. The

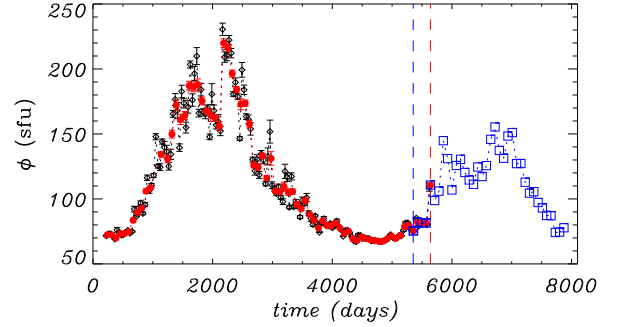


Figure 1. Radio flux averaged over the analysed time series (72-day for MDI and HMI and 36-day for GONG in black, blue and red respectively). The time is in Julian Day - 2450000 and covers most of solar cycle 23 and 24. The error bars represent the error of the mean. For HMI, they are equal to or smaller than the size of the square. The blue and red dashed vertical lines corresponds to the first date of HMI and last of MDI respectively, showing the overlapping between the data sets.

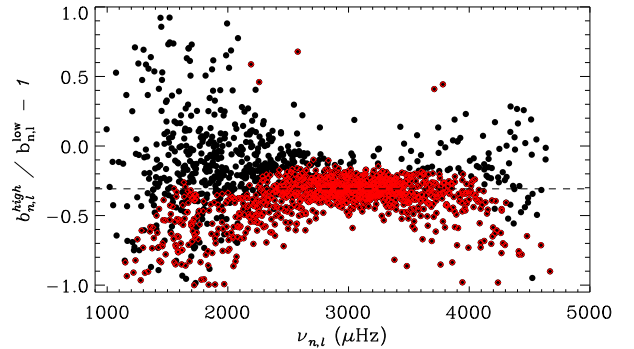


Figure 2. The figure shows the relative difference between the slope of a linear fit to each mode frequency observed by MDI as a function of radio flux using only the lower half and higher half of the radio flux. Modes which have a relative difference higher than 1.5σ , which correspond to 65% of the modes are shown in red.

relative difference is larger than 1.5σ for 65% of the modes (marked in red). The relative difference weighted mean is -0.308 ± 0.002 (dashed line). These modes are distributed around $2900 \mu\text{Hz}$ with a FWHM of $1000 \mu\text{Hz}$. Using HMI data, I get similar results as MDI, despite the smaller range in the observed radio flux, but considering the better quality of data than MDI. For the GONG data, the absolute relative difference weighted mean is 54% larger than MDI (-0.473 ± 0.002), and the relative difference is larger than 1.5σ for 80% of the modes. Although I am using GONG data for the same time period as MDI, GONG frequencies are obtained every 36 days, which is half of MDI time series, thus there are twice as many data points than MDI. The slope decrease with solar activity is also shown in Figure 3 for three individual modes. Linear regression of individual mode frequencies is performed over subsets of fifty-sfu radio-flux intervals, and each subset is displaced by twenty-sfu from the previous one.

I propose a Gompertz model to represent the frequency

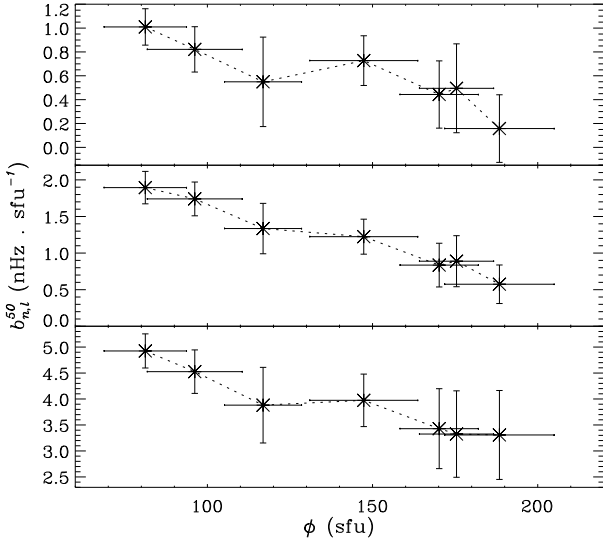


Figure 3. Variation of the slope of the frequency variation with radio flux observed by MDI averaged over intervals of fifty-sfu for three different modes. The horizontal and vertical error bars are the standard deviation of the mean radio flux and the slope, respectively. From top to bottom panel, the modes are: $n=0$, $l=247$, $\nu = 1583 \mu\text{Hz}$; $n=3$, $l=112$, $\nu = 2240 \mu\text{Hz}$; $n=13$, $l=39$, $\nu = 3330 \mu\text{Hz}$. The slope increases with mode frequency (from top to bottom panel).

variation with solar activity instead of a linear fit. The Gompertz model is a frequently used sigmoid function, especially in biological and social sciences. It has been often used to model biological ageing or the growth of plants, animals, bacteria and even tumour, but it has also been used on other research fields such as Business, Computer Science, Engineering, Geophysics, and Physics. The growth rate is quick at first, but eventually, it slows down and then levels off. Numerous parametrization of the Gompertz model can be found in the literature. I use here the one given by Tjorve & Tjorve (2017, equation 18), where each parameter only affects one shape characteristic. The Gompertz model plus a constant term ($\nu_{n,l}^c$) was fitted to each individual mode frequency: $\nu_{n,l}(\phi)$ where ϕ is the mean radio flux at each time interval.

$$\nu_{n,l}(\phi) = A_{n,l} \exp \{ -\exp [-ek_{n,l}(\phi - \Phi_{n,l})] \} + \nu_{n,l}^c \quad (1)$$

where $\exp(x) = e^x$ and e is the base of the natural logarithm \ln . $A_{n,l}$ represents the upper asymptote, $\Phi_{n,l}$ is the radio flux at the inflection point, and $k_{n,l}$ is the maximum relative growth rate (Figure 4). The maximum absolute growth rate is given by $K_{n,l} = k_{n,l} \cdot A_{n,l}$ and it is equal to the tangent at the inflection point. The value at inflection is locked at 36.8% of the upper asymptote:

$$\nu_{n,l}(\Phi_{n,l}) = A_{n,l}e^{-1} + \nu_{n,l}^c. \quad (2)$$

The proposed Gompertz function has a physical meaning only for ϕ equal to or larger than the quiet Sun radio flux. In equation 1, when $\phi \rightarrow -\infty$, $\nu_{n,l} \rightarrow \nu_{n,l}^c$. The constant term, $\nu_{n,l}^c$, does not have a physical meaning. From the model, one can estimate the maximum possible frequency for each mode, $\nu_{n,l}^{\max}$, when $\phi \rightarrow +\infty$, $\nu_{n,l} \rightarrow \nu_{n,l}^{\max} = A_{n,l} + \nu_{n,l}^c$.

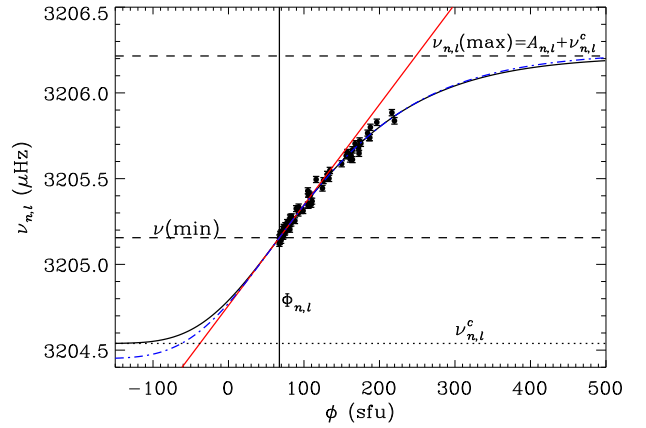


Figure 4. Example of the fitted model to the observed frequencies for a given mode: $l=85$, $n=8$ and $\nu=3205.39 \mu\text{Hz}$ (black sigmoid). The red line indicates the maximum absolute growth rate $K_{n,l}$ at the inflection point: $\Phi_{n,l} = 67.4 \text{ sfu}$ (vertical full line). The upper and lower horizontal dashed lines show the upper asymptote plus the offset term, $\nu_{n,l}^{\max}$, and the frequency corresponding to the smallest observed radio flux, $\nu_{n,l}^{\min}$, respectively. The horizontal dotted line represents the constant term, $\nu_{n,l}^c$. The blue dot-dashed sigmoid is the same as the black one but using $\Phi_{n,l} = 59 \text{ sfu}$.

The frequency shift rate decreases as the radio flux increases (Figure 3), thus the inflection point, $\Phi_{n,l}$, is at the minimum observed solar radio flux or at an even smaller value. I assume that $\Phi_{n,l}$ is the same for all modes and equal to the minimum observed solar flux in the data ($\phi^{\min}=67.4 \text{ sfu}$ for MDI and GONG). In this case, the minimum-to-maximum frequency shift is given by:

$$\Delta\nu_{n,l} = \nu_{n,l}^{\max} - \nu_{n,l}^{\min} = A_{n,l}(1 - e^{-1}), \quad (3)$$

where $\nu_{n,l}^{\min}$ is the mode frequency at $\phi = \Phi_{n,l}$. The $\Phi_{n,l}$ parameter shifts the sigmoid curve horizontally without changing its shape (Tjorve & Tjorve 2017).

Equation 1 was fitted using a Levenberg-Marquardt least-squares fit (Markwardt 2012) with only two free parameters $k_{n,l}$ and $\nu_{n,l}^c$. $\Phi_{n,l}$ is fixed at 67.4 sfu. Applying Equation 2, we have $A_{n,l} = [\nu_{n,l}^{\min} - \nu_{n,l}^c]e$, where $\nu_{n,l}(\Phi_{n,l}) = \nu_{n,l}(\phi^{\min}) = \nu_{n,l}^{\min}$. After doing a linear regression to one-third of the smallest values of the radio flux, $\nu_{n,l}^{\min}$ is given by the fitted frequency corresponding to the smallest observed radio flux. Out of 1868 modes observed by MDI, 1605 were successfully fitted indicating a success rate of 86%. The success rate is 83% and 77% for GONG and HMI respectively. HMI observations were taken during solar cycle 24 which has a smaller maximum (155 sfu) than MDI and GONG observations (220 sfu). Also, the used HMI data has a higher minimum (74 sfu) and they are not as long as MDI, there are 74 time series in MDI data against only 37 for HMI. The same value was used for HMI as for MDI and GONG for $\Phi_{n,l} = 67.4 \text{ sfu}$. The weaker Cycle 24 makes the frequency shift smaller and worsens the Gompertz fitting, specially for low-frequency modes ($\nu < 2.5 \text{ mHz}$) that have a small frequency-shift gradient.

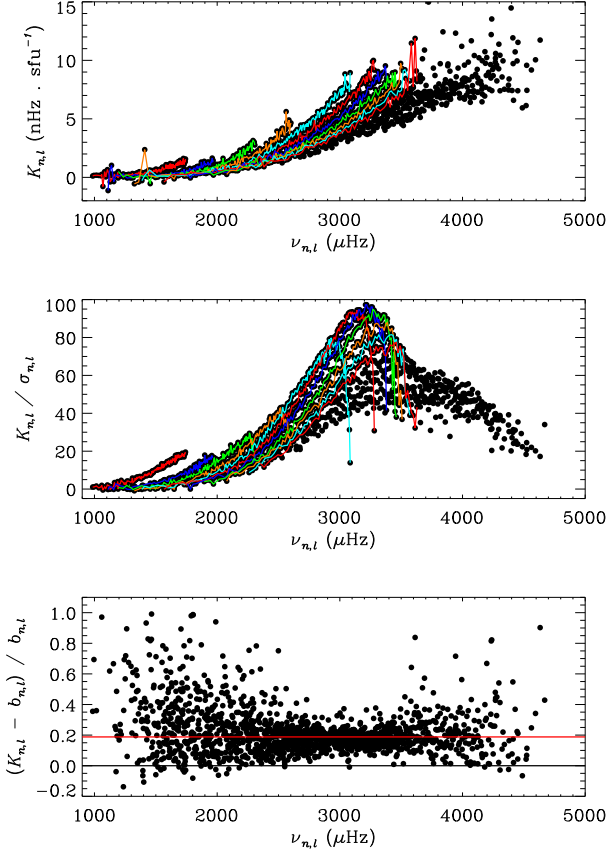


Figure 5. Top Panel. Fitted values of the maximum absolute growth rate $K_{n,l}$. Middle Panel. Fitted values of $K_{n,l}$ divided by its fitting uncertainty ($\sigma_{n,l}$). Bottom Panel. Comparison between $K_{n,l}$ and the linear fitting slope, $b_{n,l}$. The coloured lines, in the top and middle panels, show the order of the modes from $n=0$ until 10 repeating the sequence in the order red, blue, green, salmon, and cyan. The red horizontal line in the bottom panel represents the median of the relative differences.

4 RESULTS AND DISCUSSION USING MDI DATA

Figure 5 (top panel) shows the maximum absolute growth rate, $K_{n,l}$, which increases with frequency and decreases with mode order n . The fitted values are several times its fitting uncertainty ($\sigma_{n,l}$) as shown in the middle panel, except for 36% of modes which are smaller than 5σ . These modes have frequencies smaller than $2000 \mu\text{Hz}$. The bottom panel compares $K_{n,l}$ with the slope of a linear fit ($b_{n,l}$). The red horizontal line shows the median of the relative difference equal to 0.19. $K_{n,l}$ is closer to the slope fitting only radio fluxes smaller than its middle point ($b_{n,l}^{\text{low}}$ in Figure 2). In this case, the median is equal to 0.04.

Figure 6 shows the minimum-to-maximum frequency shift (Equation 3) which also increases with frequency and decreases with order n (top panel). There is scatter in its variation with n . The fitted values are several times its sigma as shown in the middle panel, except for 28% of all modes which are smaller than 5σ . The bottom panel shows the relative difference between $\Delta\nu_{n,l}$ and frequency shift obtained by the linear fit defined as $\Delta\nu_{n,l}^{\text{linear}} = b_{n,l} \cdot \Delta\phi$, where $\Delta\phi$

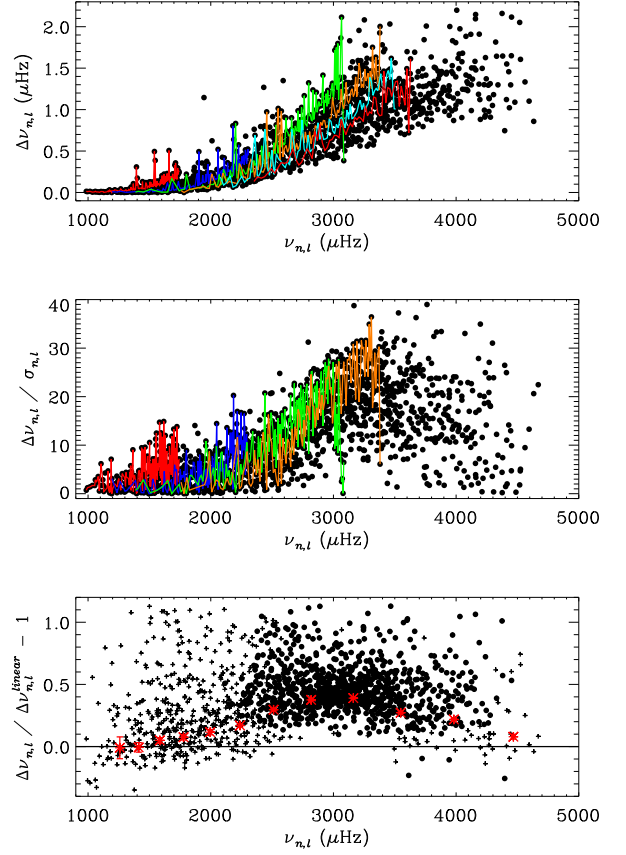


Figure 6. Top Panel. Minimum-to-maximum frequency shift, $\Delta\nu_{n,l}$ (Equation 3). Middle Panel. $\Delta\nu_{n,l}$ divided by its uncertainty ($\sigma_{n,l}$). Bottom Panel. Relative difference between $\Delta\nu_{n,l}$ and the linear frequency shift: $\Delta\nu_{n,l}^{\text{linear}} = b_{n,l} \cdot \Delta\phi$, where $\Delta\phi = 145 \text{ sfu}$. The modes which have a relative difference larger than 2σ are represented with circles instead of crosses. The red stars are weighted averages of 0.05 intervals in $\log\nu_{n,l}$ (in μHz) and their error bars are the error of the mean which is smaller than the symbol except for the first two stars. The coloured lines, in the top and middle panels, show the order of the modes from $n = 0, 2, 4, 6, 8$, and 10 which are red, blue, green, salmon, cyan, and red respectively for the top panel and only until $n=6$ for the middle panel.

$= (\phi^{\text{max}} - \phi^{\text{min}}) = 145 \text{ sfu}$ was chosen to get similar values to $\Delta\nu_{n,l}$ at lower frequencies. The observed radio-flux difference, $\Delta\phi$, for MDI is 220 sfu. The modes which have a relative difference larger than 2σ are represented with circles instead of crosses. $\Delta\nu_{n,l}$ gives the maximum frequency shift possible, while $\Delta\nu_{n,l}^{\text{linear}}$ depends on the cycle that is being analysed. Although their absolute differences are very small ($\lesssim 0.2 \mu\text{Hz}$), there is a systematic variation in the relative difference with frequency (Figure 6).

The saturation is defined as the value of radio flux, $\phi_{n,l}^{\text{sat}}$, whose corresponding mode frequency differs from $\nu_{n,l}^{\text{max}}$ by less than 0.0004% (i.e., $\lesssim 0.01 \mu\text{Hz}$ in $2500 \mu\text{Hz}$). From Equation 1, we have:

$$\phi_{n,l}^{\text{sat}} = \Phi_{n,l} - \ln \left[-\ln \left(1 - \frac{4 \times 10^{-6} \cdot \nu_{n,l}}{A_{n,l}} \right) \right] \cdot \frac{A_{n,l}}{e \cdot k_{n,l}}. \quad (4)$$

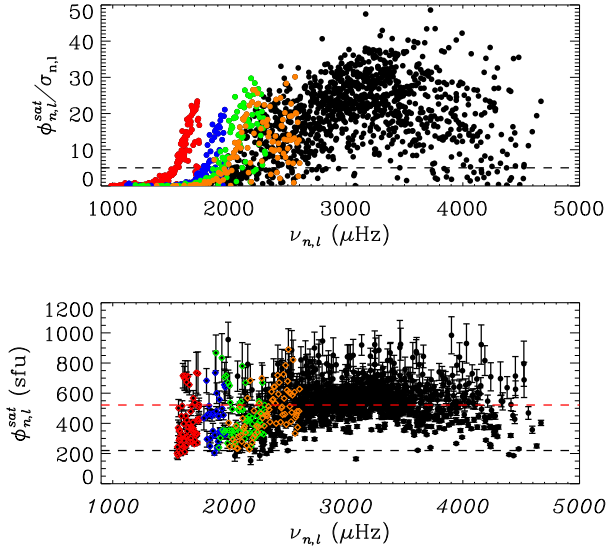


Figure 7. The mode saturation $\phi_{n,l}^{sat}$ given by Equation 4. Top Panel. Mode saturation divided by its uncertainty ($\sigma_{n,l}$). The horizontal dashed line is at 5σ . Bottom Panel. Only modes with saturation larger than 5σ . The red and black horizontal dashed lines represents the median saturation and the maximum observed radio flux by MDI and GONG. The coloured symbols, in both panels, show the order of the modes only from $n=0$ until 3 which are red, blue, green, salmon respectively.

In Figure 7 (top panel), the saturation is larger than 5σ for 77% of the modes, where the saturation uncertainty is calculated by propagation of the fitting uncertainties. The bottom panel shows only well-determined saturation (i.e., larger than 5σ). Their median saturation is 522 sfu (horizontal red dashed line) and 70% of the modes are within (522 ± 140) sfu. Their weighted mean is (428.7 ± 0.6) sfu. The largest radio flux, averaged over a 72-day, during Cycle 23 is 220 sfu (horizontal black dashed line). Half of the modes will reach saturation only if a cycle is more than two times stronger than Cycle 23. Cycle 19, the strongest cycle in the last century, during which there was 72-day radio flux average as large as 273 sfu, is only 24% stronger than Cycle 23.

The deviation from a linear fit is very small. The significance of the results is tested by adding normally distributed random numbers with a standard deviation equal to the observed frequency uncertainty, $e_{n,l}(\phi)$, to the linear fitted mode frequency, $\nu_{n,l}^{linear}(\phi) = a_{n,l} + b_{n,l} \cdot \phi$, and fitting the Gompertz model to each individual mode frequency for 1000 realizations, in the same way as the observations. The smallest median saturation over all modes, which have $\phi_{n,l}^{sat} > 5\sigma$, is 638 sfu, which is 23% larger than the observed one; and only 1% of the realizations have a median smaller than 680 sfu (i.e., 30% larger than the observed one). Thus, the results from the Gompertz model using MDI data are statistically significant.

As mentioned, it is possible that $\Phi_{n,l}$ is smaller than the minimum observed radio flux. Assuming a value for $\Phi_{n,l}$ that is 8 sfu smaller than the minimum observed by MDI (12% smaller), the Gompertz fitted parameters change by a small

amount. The mean saturation is 10.9 sfu larger than before (2.5%) and the median increases by 29 sfu (5.6%). Figure 4 shows the sigmoid for a given mode with the smaller $\Phi_{n,l}$ in blue to be compared with the previous one in black. Since 1947, the lowest observed daily radio flux is equal to 62 sfu, which happened during the 1953-1954 minimum. During the recent unusually low 2007-2008 minimum, the smallest daily value is 65 sfu.

The frequency shifts depend mostly on the mode frequency after they have been weighted by the mode inertia, $\Delta\nu_{n,l} \propto \nu_{n,l}^\alpha / I_{n,l}$, indicating that the source of the perturbations is close to the solar surface (Libbrecht & Woodard 1990). Figure 8 shows $\Delta\nu_{n,l}$ scaled by $I_{n,l}$ (top panel) and by the normalized mode inertia $Q_{n,l}$ (middle panel), expressed in base-10 logarithm. $Q_{n,l}$ is normalized by the inertia of a radial mode of the same frequency (Christensen-Dalsgaard et al. 1989). The mode inertia was obtained using model ‘S’ (Christensen-Dalsgaard et al. 1996). The linear frequency shift, $\Delta\nu_{n,l}^{linear}$, is also plotted for comparison and it is the same as defined in Figure 6, except that here $\Delta\phi = 195$ sfu was chosen to get similar values to $\Delta\nu_{n,l}$ at all frequencies. The p modes are in black and red for the Gompertz fitting (Equation 3) and linear fitting, respectively. The f modes are in blue and green respectively and have different behaviour from p modes for both fitting methods. The response of the frequency shift scaled by the mode inertia depends upon the physical mechanism responsible for changing the mode frequencies during the solar cycle (Gough 1990). Thus, although both f and p modes are well correlated with radio flux, the cause of frequency variation with solar activity are different (see, for example, Dziembowski & Goode 2005).

In Figure 8, a straight line fitting to $\log(\delta\nu_{n,l} \cdot Q_{n,l})$ in the middle panel corresponds to a parabolic-like shape in the top panel (Rabello-Soares et al. 2008, Figure 6), hence α varies with frequency. A linear regression to $\log(\Delta\nu_{n,l}^{linear} \cdot Q_{n,l})$ shows a clear change in the slope around 2500 μHz and the slopes, γ , are:

$$\begin{aligned} \gamma &= 5.97 \pm 0.02 \quad \text{for } \nu < 2500 \mu\text{Hz} \\ \gamma &= 3.57 \pm 0.01 \quad \text{for } \nu > 2500 \mu\text{Hz}. \end{aligned} \quad (5)$$

for p modes. The f modes have a larger coefficient, $\gamma = 7.90 \pm 0.06$. As pointed out by Chaplin et al. (2001), the upper turning point of the modes gets deeper as the mode frequency decreases and, around 2500 μHz , the gradient becomes suddenly an order of magnitude larger than before and low-frequency modes are reflected back at much deeper layers of the solar atmosphere, which might affect the frequency shift since it is expected that the source of perturbation is close to the surface. Although there is a good agreement between both frequency shifts, the logarithm of the ratio between Gompertz and linear frequency shift is plotted in the bottom panel, where f and p modes are the blue and black small circles respectively. The red circles are weighted averages in 0.05-log ν μHz intervals. They show a clear difference between the two fitting methods. Fitting a straight line to $\log \Delta\nu_{n,l} / \Delta\nu_{n,l}^{linear}$, one gets $\Delta\gamma = \gamma_{\text{Gompertz}} - \gamma_{\text{linear}}$:

$$\begin{aligned} \Delta\gamma &= 0.40 \pm 0.04 \quad \text{for } \nu < 2500 \mu\text{Hz} \\ \Delta\gamma &= -0.31 \pm 0.02 \quad \text{for } \nu > 2500 \mu\text{Hz}. \end{aligned} \quad (6)$$

The Gompertz fitting estimates a slightly different behaviour

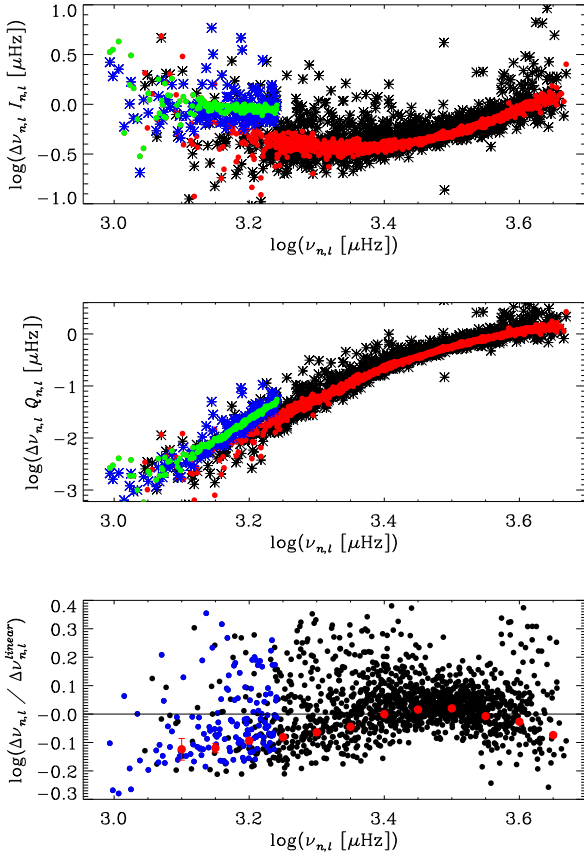


Figure 8. The frequency shift, $\Delta\nu_{n,l}$, scaled by $I_{n,l}$ (top panel) and by the normalized mode inertia $Q_{n,l}$ (middle panel), expressed in base-10 logarithm. The p (f) modes are in black and red (blue and green) for the Gompertz frequency shift (Equation 3) and the linear frequency shift, $\Delta\nu_{n,l}^{\text{linear}}$ (using $\Delta\phi = 195$ sfu), respectively. The logarithm of the ratio between Gompertz and linear frequency shift is plotted in the bottom panel, where f and p modes are the blue and black small circles respectively. The red circles are weighted averages in $0.05\text{-log } \nu$ μHz intervals.

for the scaled frequency shift than the linear fitting, where γ is larger by 7% and smaller by 9% for frequencies smaller and larger than $2500 \mu\text{Hz}$ respectively.

5 RESULTS AND DISCUSSION USING HMI AND GONG DATA

GONG. The saturation weighted mean, calculated using Equation 4, is (395.4 ± 0.3) sfu, which is similar to the one obtained using MDI data, it is 8% smaller than MDI. The median saturation, calculated using modes with saturation larger than 5σ (which corresponds to 86% of the fitted modes), is 434 sfu and 17% smaller than MDI. Similarly to MDI, I fitted the Gompertz model to the linear fitted GONG mode frequencies after adding normally distributed random numbers with a standard deviation equal to the uncertainty of the GONG observed frequencies to test the significance of the results. For 1000 realizations, the smallest median saturation is 858 sfu, using only modes with saturation larger than 5σ , which is almost twice the median of the observa-

tions. The results from the Gompertz model using GONG data are even more robust than for MDI. For GONG, there are twice as many points as for MDI during the same time period due to the shorter time series (36-day) that the frequencies were obtained.

HMI. The saturation weighted mean, calculated using Equation 4 with $\Phi_{n,l}=67.4$ sfu same as for MDI, is (226.7 ± 0.3) sfu, which is almost half the saturation obtained using MDI data. The median saturation, calculated using modes with saturation larger than 5σ (which corresponds to 74% of the fitted modes), is 281 sfu. There is no significant change in the saturation determination for HMI using $\Phi_{n,l} = 74$ sfu, which is observed minimum radio flux for the HMI data used here. Repeating the Monte Carlo simulation for HMI data, using only modes with saturation larger than 5σ , the smallest median saturation is 200 sfu, which smaller than the observed median. There are 18 realizations with a median smaller than the observed one and 85 with a weighted mean smaller than the observed one. The Gompertz fitting using HMI data is not statistically significant. The results are due to the randomness introduced by observed frequency uncertainties. Cycle 24 is among the weakest cycles in the last 200 years, As the frequency shift is far from saturation, it is not possible to determine it. The saturation obtained for MDI and GONG could be a lower limit for the true saturation. A stronger cycle is needed to get a better determination.

6 CONCLUSIONS

It is shown that the rate at which the frequency increases with the solar radio flux decreases as the solar radio flux increases using MDI, HMI and GONG data. A sigmoid function is proposed instead of a linear fit to the frequency dependence with solar radio flux: the Gompertz model as defined by Tjorve & Tjorve (2017) plus a constant (Equation 1).

Although the deviation from a linear fit is small, it is shown that the sigmoid fitting is statistically significant using MDI and GONG data. This is not the case for HMI data, which was obtained during solar Cycle 24, a much weaker cycle than the previous one when MDI and GONG data were taken. Using MDI and GONG data, I estimate a saturation level of four-hundred sfu averaging over all modes, which is 50% larger than Cycle 19, the strongest cycle in the last century. The saturation observed by GONG is a few percents lower than by MDI. The exact mechanism causing the frequencies to increase with solar activity is not precisely known, which makes it difficult to speculate on why they increase at a smaller rate at high activity levels indicating a possible saturation at a high enough activity level.

The minimum-to-maximum frequency difference scaled by the normalized mode inertia obtained here has different behaviour than the commonly used difference between the frequencies obtained at or close to the cycle maximum activity and to its minimum (i.e., assuming a linear fit). The slope is 7% larger and 9% smaller than assuming a linear fit for with frequency smaller and larger than $2500 \mu\text{Hz}$, respectively. This dissimilarity in the response is a direct consequence of the nature of the perturbation causing the frequency variation and, although small, it should not be neglected.

ACKNOWLEDGEMENTS

This research was supported in part by Minas Gerais State Agency for Research and Development (FAPEMIG), Brazil.

Solar radio flux data is provided by the National Resources Canada (NRC) Space Weather. MDI data is provided by the SOHO/MDI consortium. SOHO is a project of international cooperation between ESA and NASA. HMI data is provided by NASA/SDO and HMI science team. This work utilizes data obtained by the Global Oscillation Network Group (GONG) program, managed by the National Solar Observatory, which is operated by AURA, Inc. under a cooperative agreement with the National Science Foundation. The data were acquired by instruments operated by the Big Bear Solar Observatory, High Altitude Observatory, Learmonth Solar Observatory, Udaipur Solar Observatory, Instituto de Astrofísica de Canarias, and Cerro Tololo Inter-american Observatory.

REFERENCES

- Broomhall A.-M., Nakariakov V. M., 2015, *Sol. Phys.*, **290**, 3095
 Brun A. S., Browning M. K., 2017, *Living Reviews in Solar Physics*, **14**, 4
 Chaplin W. J., Appourchaux T., Elsworth Y., Isaak G. R., New R., 2001, *MNRAS*, **324**, 910
 Christensen-Dalsgaard J., Thompson M. J., Gough D. O., 1989, *MNRAS*, **238**, 481
 Christensen-Dalsgaard J., et al., 1996, *Science*, **272**, 1286
 Covington A. E., 1969, *J. R. Astron. Soc. Canada*, **63**, 125
 Dziembowski W. A., Goode P. R., 2005, *ApJ*, **625**, 548
 Fleck B., Couvidat S., Straus T., 2011, *Sol. Phys.*, **271**, 27
 García R. A., Mathur S., Salabert D., Ballot J., Régulo C., Metcalfe T. S., Baglin A., 2010, *Science*, **329**, 1032
 Goldreich P., Murray N., Willette G., Kumar P., 1991, *ApJ*, **370**, 752
 Gough D. O., 1990, in Osaki Y., Shibahashi H., eds, *Lecture Notes in Physics*, Berlin Springer Verlag Vol. 367, Progress of Seismology of the Sun and Stars. p. 283, doi:10.1007/3-540-53091-6
 Harvey J. W., et al., 1996, *Science*, **272**, 1284
 Hill F., et al., 1996, *Science*, **272**, 1292
 Jain K., Tripathy S. C., Hill F., 2009, *ApJ*, **695**, 1567
 Kiefer R., Schad A., Davies G., Roth M., 2017, *A&A*, **598**, A77
 Kiefer R., Komm R., Hill F., Broomhall A.-M., Roth M., 2018, *Sol. Phys.*, **293**, 151
 Larson T. P., Schou J., 2015, *Sol. Phys.*, **290**, 3221
 Larson T. P., Schou J., 2018, *Sol. Phys.*, **293**, 29
 Li L. H., Basu S., Sofia S., Robinson F. J., Demarque P., Guenther D. B., 2003, *ApJ*, **591**, 1267
 Libbrecht K. G., Woodard M. F., 1990, *Nature*, **345**, 779
 Markwardt C., 2012, MPFIT: Robust non-linear least squares curve fitting, Astrophysics Source Code Library (ascl:1208.019)
 Mullan D. J., MacDonald J., Townsend R. H. D., 2007, *ApJ*, **670**, 1420
 Rabello-Soares M. C., 2011, *Journal of Physics Conference Series*, **271**, 012026
 Rabello-Soares M. C., Korzennik S. G., Schou J., 2008, *Advances in Space Research*, **41**, 861
 Santos A. R. G., et al., 2018, *ApJS*, **237**, 17
 Scherrer P. H., et al., 1995, *Sol. Phys.*, **162**, 129
 Schonfeld S. J., White S. M., Henney C. J., Arge C. N., McAteer R. T. J., 2015, *ApJ*, **808**, 29
 Schou J., et al., 2012, *Sol. Phys.*, **275**, 229
 Tapping K. F., 1987, *J. Geophys. Res.*, **92**, 829

- Tjorve K. M. C., Tjorve E., 2017, *PLOS ONE*, **12**, 1
 Usoskin I. G., 2017, *Living Reviews in Solar Physics*, **14**, 3
 Woodard M. F., Noyes R. W., 1985, *Nature*, **318**, 449

This paper has been typeset from a \TeX / \LaTeX file prepared by the author.